ACS OMEGA

http://pubs.acs.org/journal/acsodf

Article

# Bulk Molybdenum and Tungsten Phosphides for Selective Phenol Production from Guaiacol

Maria A. Golubeva,* Mariyam Mukhtarova, Alexey A. Sadovnikov, and Anton L. Maximov

Cite This: *ACS Omega* 2022, 7, 40586−40595

Read Online

ACCESS | Metrics & More | Article Recommendations | Supporting Information

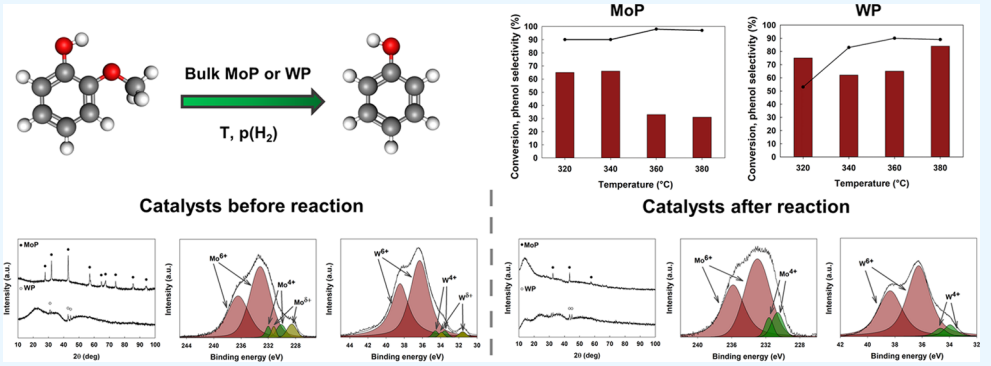


**ABSTRACT:** Bulk MoP and WP were investigated and compared in guaiacol hydrodeoxygenation to phenol. The catalysts obtained were studied by X-ray diffraction (XRD), X-ray photoelectron spectroscopy (XPS), scanning electron microscopy (SEM), and temperature-programmed desorption of $NH_3$ ($NH_3$-TPD) analyses. MoP was shown to be more active than WP. However, WP was more selective in phenol production. Guaiacol conversion using MoP was 90−98%. The highest selectivity for phenol was 66% (340 °C). By increasing the temperature to 380 °C, phenol selectivity decreased to 31%, while selectivity for cyclohexane increased to 29%. Thus, MoP was active not only in hydrodeoxygenation but also in hydrogenation. Guaiacol conversion over WP was 53−90%. The highest selectivity for phenol was 84% (380 °C). Hydrogenation products were also detected but with low selectivity. Thus, WP was active in the partial hydrodeoxygenation of guaiacol and was more suitable for the selective production of phenol than MoP. It was shown that after a 30 h recycling test, the activity of MoP did not decrease (1st and 5th cycle conversion value was 91%), while the activity of WP reduced (1st and 5th cycle conversion values were 81 and 64%, respectively). However, the activity of both catalysts at average conversion values decreased. Selectivity for phenol remained unaltered over both catalysts. It was supposed that catalyst activity decreased due to partial destruction of the crystalline phosphide phase and the surface phosphide oxidation to phosphate.

## 1. INTRODUCTION

The growing interest of the world community in biomass processing into fuels and chemicals is due to both biomass carbon neutrality and its wide availability.[1,2] Lignocellulosic biomass mainly consists of polysaccharides (cellulose and hemicelluloses) and the phenolic polymer lignin. Lignin is a primary biosource of aromatic structures.[3] Various types of phenolic compounds, ethers, and aromatic hydrocarbons are formed in the thermal or catalytic degradation of lignin. One of the principal resulting products is guaiacol (2-methoxyphenol).[4,5] Valuable substances such as phenol, cyclohexanol, cyclohexanone,[6,7] benzene−toluene−xylene (BTX) fraction,[8] etc., can be obtained by guaiacol processing.

Catalyst selection for guaiacol conversion plays a significant role. Noble metals, such as Pt, Pd, Ru, and Rh, demonstrate high activity under mild conditions.[9−12] However, their use is unattractive due to the high cost. The cost of transition metal sulfide catalysts is much lower; nevertheless, they are characterized by deactivation on account of sulfur leaching and oxide formation.[13,14] Lately, transition metal phosphides, such as nickel, molybdenum, and tungsten, have been successfully applied for hydroprocessing of bio-derived phenolic compounds and show high activity.[15−19] Nevertheless, MoP and WP in comparison with $Ni_2P$ still remain insufficiently explored in this process. So far, MoP and WP have been mainly used in the hydrodeoxygenation of vegetable oils and their derived compounds.[20−25]

Received: October 3, 2022
Accepted: October 18, 2022
Published: October 27, 2022

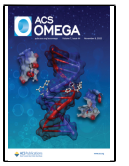





https://doi.org/10.1021/acsomega.2c06396
*ACS Omega* 2022, 7, 40586−40595

There are several reports on the hydrodeoxygenation of phenols using transition metal phosphides including MoP and WP. For example, Zhao et al.[26] carried out a comparison of silica-supported $Ni_2P$, $Co_2P$, $Fe_2P$, MoP, and WP in guaiacol hydrodeoxygenation. Guaiacol conversion was measured in a packed bed reactor at 300 °C, atmospheric pressure, a contact time of 20.2 min, and a space velocity of 1.4 $h^{-1}$ and was changed for catalysts as follows: $Ni_2P/SiO_2$ (80%) > $Co_2P/SiO_2$ (70%) > $Fe_2P/SiO_2$ (64%) > $WP/SiO_2$ (60%) > $MoP/SiO_2$ (54%). Phenol and benzene were the main reaction products. Phenol was obtained with 100% selectivity over $WP/SiO_2$. Benzene selectivity was reduced in a row: $Ni_2P/SiO_2$ (60%) > $MoP/SiO_2$ (53%) > $Co_2P/SiO_2$ (52%). Ouyang et al.[18] studied 2-metoxy-4-propylphenol transformation in a fixed-bed reactor at 350 °C, 90 bar, 30 mL/min $H_2$, WHSV = 80 $h^{-1}$. Substrate conversion follows the order $MoP/SiO_2$ (98%) > $CoP/SiO_2$ (84%) > $Ni_2P/SiO_2$ (77%) > $WP/SiO_2$ (48%) > $FeP/SiO_2$ (4%). The best 4-propylphenol selectivity of 90% was observed for $MoP/SiO_2$. Some reports are devoted to phenol hydrodeoxygenation.[19,27] Inocêncio et al.[19] investigated benzene selectivity at low phenol conversion (300 °C, 1 atm, a fixed-bed reactor). It was changed as follows: $Ni_2P$ (94.6%) > CoP (84.2%) > WP (82.7%) > FeP (75.3%) > MoP (57.5%). Berenguer et al.[27] made a comparison of $Ni_2P$, $Co_2P$, and MoP supported on Al-SBA-15, m-$Al_2O_3$ (mesoporous $\gamma$-$Al_2O_3$), and CMK-3 (ordered mesoporous carbon) activity in an autoclave reactor at 220 °C, 40 bar $H_2$, for 2 h. $Ni_2P$/Al-SBA-15, $Ni_2P$/m-$Al_2O_3$, and $Co_2P$/m-$Al_2O_3$ were shown to convert phenol fully. $Ni_2P$/Al-SBA-15 also demonstrated the highest activity (93%) in phenol hydrodeoxygenation, while MoP/Al-SBA-15, MoP/m-$Al_2O_3$ (65%), MoP/Al-SBA-15 (56%), and MoP/CMK-3 (54%) showed moderate hydrodeoxygenation activity. Whiffen et al.[28] carried out an investigation into the influence of the bulk MoP synthesis method on its activity in p-cresol hydrodeoxygenation (350 °C, 4.4 MPa $H_2$, 5 h, a stirred batch reactor). A citric acid additive was shown to increase the surface area and dispersion of the catalyst. MoP-CA (71%) calcined at 550 °C contributed more to higher p-cresol conversion than MoP-noCA (45%). Despite this fact, toluene and methylcyclohexane selectivities on these catalysts were comparable (51 and 47% using MoP-CA and 49 and 50% using MoP-noCA, respectively).

The present work carries out an investigation into bulk molybdenum and tungsten phosphides in guaiacol hydrodeoxygenation. The absence of a support is assumed to provide better access of substrate molecules to the catalyst active sites. A comparison of the bulk MoP and WP catalytic activity in guaiacol hydrodeoxygenation is carried out for the first time. Phenol is shown to be the main product of this process. Guaiacol conversion was higher using MoP (98%); however, WP was more selective for the production of phenol (selectivity reached 84%).

## 2. EXPERIMENTAL SECTION

**2.1. Catalyst Synthesis.** For molybdenum phosphide synthesis, 5.2 g of hypophosphorous acid ($H_3PO_2$, 50 wt % in water, Sigma-Aldrich) and 7.1 g of ammonium molybdate ($(NH_4)_6Mo_7O_{24}\cdot 4H_2O$, >98%, Chimmed) were dissolved in 100 mL of deionized water. The mixture was heated with magnetic stirring to remove water. Then, the solid residue was dried in an oven at 120 °C and calcined in a muffle furnace at 500 °C for 6 h. The precursor reduction to MoP was carried out at 650 °C for 6 h in a stream of $H_2$ (≥98%, Air Liquide). The resulting material was first washed with deionized water, then with ethanol (>99%, Reachem), and finally with acetone (>99.5%, Component-reaktiv) to remove impurities (e.g., unreacted precursors). Molybdenum phosphide was separated by centrifugation at 5000 rpm and dried by Ar (≥98%, Air Liquide).

Tungsten phosphide was prepared similarly; 3.1 g of $H_3PO_2$ and 6.1 g of ammonium metatungstate ($(NH_4)_6H_2W_{12}O_{40}\cdot xH_2O$, ≥99% $WO_3$, Fluka) were used. The precursor reduction was carried out at 750 °C for 6 h in a stream of $H_2$.

**2.2. Catalytic Tests.** To carry out catalytic experiments, 40.6 mg of MoP or 68.7 mg of WP, 2 g of a 10 wt % guaiacol solution in dodecane, and a magnetic anchor were placed in a stainless-steel batch reactor. The reactor was sealed and filled with $H_2$ to 5 MPa. Reactions were carried out at 320−380 °C for 6 h. After the reaction, the reactor was cooled to room temperature and then depressurized. The catalysts were separated from reaction products by centrifugation at 5000 rpm. Then, the catalysts were washed with acetone and dried by Ar.

The recycling catalytic tests were carried out in a similar way within five runs at 340 °C, 5 MPa, and 6 h for both catalysts. Also, the recycling tests were carried out at average conversion for MoP (340 °C, 5 MPa, 1 h) and for WP (360 °C, 5 MPa, 3 h).

**2.3. Characterization.** A number of physicochemical methods characterized the catalysts obtained. The powder X-ray diffraction (XRD) of the fresh and spent catalysts was carried out on a Rigaku Rotaflex D/MAX-RC X-ray diffractometer (Japan). The measurement was made in continuous scanning mode with a scanning rate of 1°/min, an angle range of 10−100°, and a scanning step of 0.04°. The phase composition was determined using an ICDD PDF-2 reference database into powder diffraction patterns. The crystallinity degree was calculated using MDI Jade 6 software. Crystallite sizes were estimated by the Scherrer equation.

X-ray photoelectron spectroscopy (XPS) of the fresh catalysts was performed using a modernized ES−2403 SDB IAI RAS electron spectrometer (Russia) equipped with a Specs GmbH PHOIBOS 100-5MCD energy analyzer (Germany) and an Al $K_\alpha$ X-ray source. The integral maximum in the C 1s spectra ($E_b$ = 284.8 eV) from the carbon contamination was used as an internal standard. Spectra were obtained using SpecLab2 software. XPS of the spent catalysts was performed using a PREVAC EA15 electron spectrometer (Poland) and an Al $K_\alpha$ X-ray source. The integral maximum in the C 1s spectra ($E_b$ = 284.8 eV) was used as an internal standard. Spectra were obtained using CasaXPS software. The spectra were deconvoluted using PeakFit Software.

Scanning electron microscopy (SEM) with energy-dispersive X-ray spectroscopy (EDX) was performed using a Carl Zeiss NVision 40 microscope (Germany) equipped with an Oxford Instruments X-Max EDX detector (U.K.) operated at 20 kV. The temperature-programmed desorption of $NH_3$ ($NH_3$-TPD) was performed using a UNISIT USGA-101 (Russia) gas chemisorption analyzer.

Gas chromatography−mass spectrometry (GC−MS) determined the qualitative composition of reaction products on a Thermo Scientific ISQ 7000 GC−MS system equipped with a Restek 5XI-17SIL MS CAP capillary column (30 m × 0.25 mm × 0.25 μm), with helium being used as a carrier gas.

Gas−liquid chromatography (GLC) defined the quantitative composition of reaction products. GLC was performed using a


https://doi.org/10.1021/acsomega.2c06396
ACS Omega 2022, 7, 40586−40595

Crystallux-4000M gas chromatograph (Russia) equipped with a flame ionization detector and an Optima-1 capillary column (25 m × 0.32 mm × 0.35 μm), with helium being used as a carrier gas. Guaiacol conversion and product selectivity were calculated by the following equations

$$\text{conversion (\%)} = \frac{\text{(mole of guaiacol consumed)}}{\text{(initial mole of guaiacol)}} \times 100\%$$

$$\text{selectivity (\%)} = \frac{\text{(mole of product formed)}}{\text{(mole of guaiacol consumed)}} \times 100\%$$

## 3. RESULTS AND DISCUSSION

**3.1. Characterization of the Fresh Catalysts.** The phase composition of the samples obtained was determined by powder X-ray diffraction analysis (Figure 1). MoP and WP

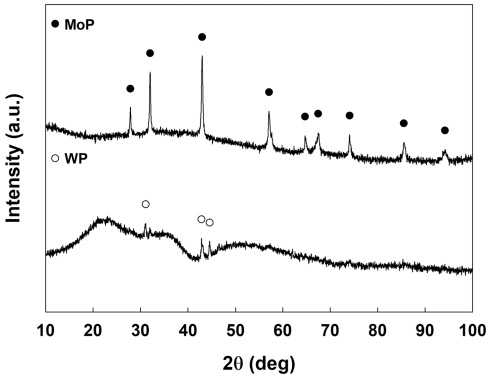


**Figure 1.** Powder X-ray diffraction of the fresh molybdenum and tungsten phosphides.

catalysts had both the amorphous phase and the crystalline component. However, MoP was more crystalline than WP. The crystallinity degree of MoP was 28% and that of WP was 13%. McEnaney et al. reported obtaining amorphous molybdenum phosphide at 600 °C. The patterns of crystalline phosphide were observed at 700 °C.[29] For tungsten phosphide, the temperature at which crystalline WP appear was 800 °C.[30] In the current work, reduction temperatures were 650 and 750 °C, respectively. Peaks were identified in the molybdenum phosphide sample at $2\theta$ = 27.84, 32.00, 42.96, 57.08, 64.68, 67.44, 74.08, 85.48, and 94.16°, corresponding to the (001), (100), (101), (110), (111), (102), (201), (112), and (202) planes in MoP (PDF No. 89-5110). The average crystallite size was 26 ± 3 nm. In the sample of tungsten phosphide, WP phase (PDF No. 80-0238) peaks were determined at $2\theta$ = 31.08, 42.84, and 44.56°, corresponding to the (011), (112), and (211) planes. The average crystallite size was 35 ± 2 nm.

The surface states of phosphides were determined using X-ray photoelectron spectroscopy. There are three valence states of Mo in the Mo 3d region spectrum (Figure 2a). The binding energies related to $Mo^{\delta+}$ and corresponding to MoP[31,32] are located at 228.6 eV ($3d_{5/2}$) and 231.2 eV ($3d_{3/2}$). The values of 230.1 and 232.0 eV are attributed to the $Mo^{4+}$ state in Mo $3d_{5/2}$ and Mo $3d_{3/2}$ regions, respectively. This state can be associated with $MoO_2$ or phosphate in the corresponding oxidation state.[32,33] The binding energies of 233.2 and 236.4 eV can be assigned to the $Mo^{6+}$ state ($MoO_3$ or phosphate) in Mo $3d_{5/2}$ and Mo $3d_{3/2}$ regions, respectively.[33−35] There are also three valence states of W in the W 4f region spectrum (Figure 2c). The peaks located at 31.6 eV ($4f_{7/2}$) and 33.9 eV ($4f_{5/2}$) can be attributed to $W^{\delta+}$ species in WP.[36,37] The values of 33.6 eV ($4f_{7/2}$) and 34.6 eV ($4f_{5/2}$) refer to $W^{4+}$ in $WO_2$.[36,37] Two other peaks are centered at 36.3 and 38.5 eV corresponding to $W^{6+}$ in W $4f_{7/2}$ and $4f_{5/2}$ regions, respectively, and can be identified as the $WO_3$ phase or tungsten phosphate.[36−38] The P spectra of MoP (Figure 2b) and WP (Figure 2d) were deconvoluted into four peaks in both cases. The binding energies of 129.9/131.1 and 129.4/130.8 eV are associated with the $P^{\delta-}$ state in MoP and WP in P $2p_{3/2}$ and $2p_{1/2}$ regions, respectively.[36] The peaks located at 134.2/135.4 and 134.2/135.3 eV refer to the oxidized $P^{5+}$ state in MoP and WP, respectively.[36] Numerical data calculated from the deconvoluted spectra are presented in Table S1. The percentage content of metal active sites $M^{\delta+}$ (M = Mo, W) on the surface of MoP was found to be higher than that on the surface of WP. The high content of oxidized species on the catalyst surface may be due to the incomplete reduction of the precursors.[39]

Scanning electron microscopy was used to observe the morphology of catalysts (Figure 3). Both samples show bulk morphology. WP particles are demonstrated to have a more regular shape than MoP particles. Energy-dispersive X-ray spectroscopy was applied to define the elemental content. The MoP catalyst was found to have an average Mo/P ratio equal to 1.1. This value is close to the stoichiometric ratio in the MoP phase. There was an average W/P ratio of 0.96 in the WP catalyst, which is also close to the stoichiometric ratio in the WP phase. In addition, oxygen was detected in both samples (O/P was 3.9 in MoP and 4.6 in WP). Its presence may be due to surface oxidation of the sample or incomplete precursor reduction.[40,41]

The $NH_3$-TPD method evaluated the acidity of the phosphide catalyst (Figure S1). For the MoP catalyst, the desorption peaks of $NH_3$ were centered at 158 and 270 °C and were related to weak and medium acid sites, respectively. The amount of $NH_3$ desorbed was evaluated as 29 μmol/g. For the WP catalyst, one desorption peak of $NH_3$ centered at 247 °C was observed. It was associated with weak acid sites.[42] The amount of $NH_3$ desorbed was evaluated as 2 μmol/g. Thus, MoP acidity was higher than the acidity of WP.

**3.2. Catalytic Activity.** The effect of temperature on the activity of MoP and WP in the hydrodeoxygenation of guaiacol was investigated. The conversion of guaiacol over MoP increased slightly with increasing temperature and was the most at 360 °C (98%, Figure 4a). At 320 and 340 °C, phenol was the main reaction product. The highest phenol selectivity, equal to 66%, was achieved at 340 °C. With increasing temperature, phenol selectivity decreased to 31% (380 °C), while cyclohexane selectivity increased. This regularity is related to the fact that the deoxygenation and hydrogenation activity of MoP increased at higher temperatures. The remaining products formed from guaiacol were anisole, cresols, toluene, and cyclohexene (Figure S2).

Proposed reaction pathways using phosphide catalysts are presented in Scheme 1. At lower temperatures, anisole, cresols, and cyclohexane were formed over MoP, in addition to phenol. Phenol was formed directly from guaiacol by demethoxylation and also by demethylation of anisole.[43,44] Cresols were formed by the isomerization of anisole.[45] Cyclohexane can be obtained from phenol in several steps. The main intermediates in the conversion of phenol to cyclohexane are benzene and cyclohexanol.[17,44,46] However, none of these products were


https://doi.org/10.1021/acsomega.2c06396
ACS Omega 2022, 7, 40586−40595

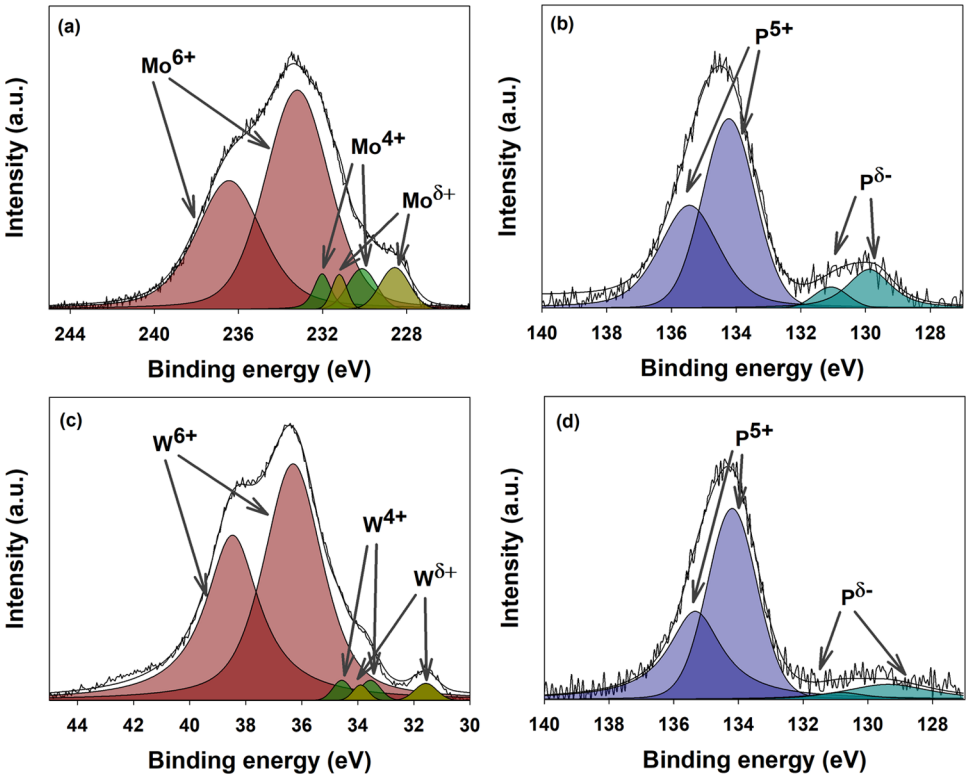


**Figure 2.** X-ray photoelectron spectra of the fresh molybdenum phosphide for (a) Mo 3d and (b) P 2p regions and tungsten phosphide for (c) W 4f and (d) P 2p regions.

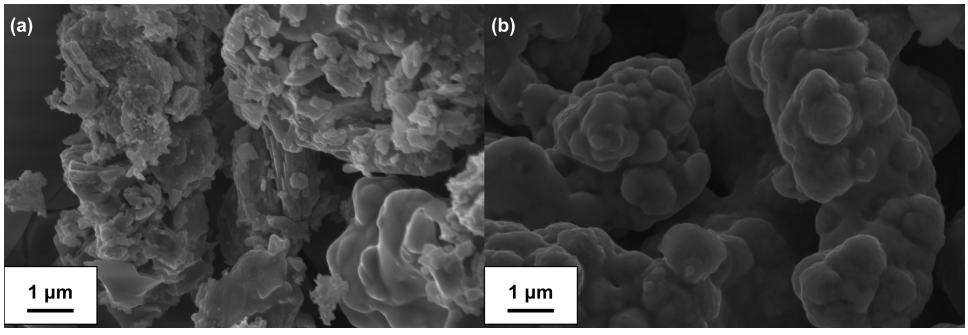


**Figure 3.** SEM images of the fresh (a) molybdenum and (b) tungsten phosphides.

found at any temperature. At 380 °C, cyclohexene was identified among the reaction products, which was an intermediate product of the phenol conversion to cyclohexane. It could be formed by the hydrogenation of benzene or the deoxygenation of cyclohexanol.[47,48] However, neither benzene nor cyclohexanol was detected. Also, at temperatures of 340−380 °C, toluene was found. It can be obtained by deoxygenation of cresols. There was no further conversion of toluene to methylcyclohexane, so it could be assumed that the intermediate product of the formation of cyclohexane from phenol was cyclohexanol, not benzene.

The conversion of guaiacol using WP increased with increasing reaction temperature and reached 90% at 360 °C (Figure 4b). In this case, with increasing temperature, selectivity for phenol first decreased and then increased to 84% at 380 °C. The rest of the reaction products were the same as when using MoP as a catalyst (Figure S3). Thus, MoP at higher temperatures was more active in hydrogenation and full hydrodeoxygenation, while WP was more selective to the formation of phenol. Such differences in the activity of the catalysts can be associated with the differences in the catalyst properties, identified by the XPS and $NH_3$-TPD techniques. Various active sites are distinguished on the surface of transition metal phosphide catalysts. Brønsted ($PO_x$−H) and Lewis ($M^{x+}$, $M^{\delta+}$) acid sites are responsible for acid-catalyzed transformations and metal ($M^{\delta+}$) sites are responsible for hydrogenation.[40,41,49] According to the XPS data (Table S1), there are more metal sites on the surface of MoP than those on the surface of WP. This fact may explain the formation of a larger amount of hydrogenation products, including cyclohexane, when MoP was used. The higher acidity of MoP estimated by $NH_3$-TPD contributes to the higher conversion of guaiacol as well as to the formation of full deoxygenation products.[49,50]

**3.3. Recycling Test.** To estimate the stability of catalysts, the recycling test of five runs (30 h) was carried out. The stability was studied under similar conditions for both catalysts: 340 °C, 5 MPa, and 6 h. Guaiacol conversion over


https://doi.org/10.1021/acsomega.2c06396
ACS Omega 2022, 7, 40586−40595

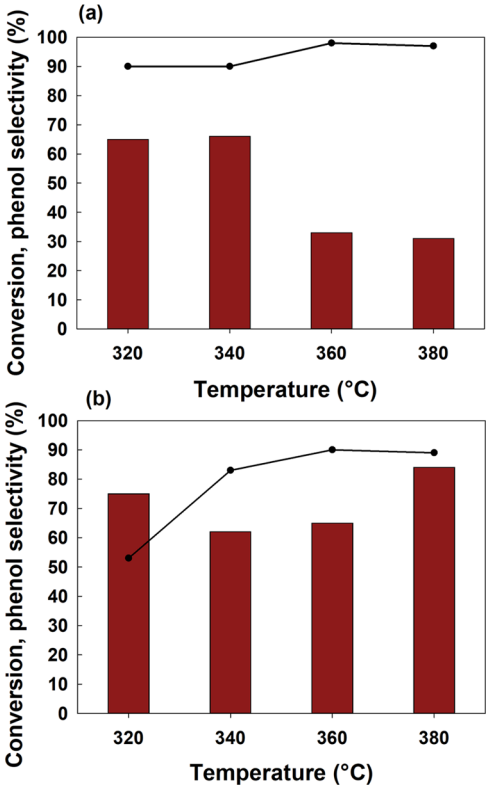


**Figure 4.** Effect of reaction temperature on guaiacol conversion and phenol selectivity over (a) MoP and (b) WP catalysts.

MoP was shown to be about 90% within five cycles (Figure 5a). Selectivity for phenol decreased insignificantly and was 60−66%. Guaiacol conversion over WP reduced from 81% on the 1st test run to 64% on the 4th and 5th test runs, while phenol selectivity remained 64−66% (Figure 5b). Thus, under the selected reaction conditions, a decrease in activity was noted only for WP. The stability of MoP was evaluated at high conversion close to quantitative, so the decrease in activity could be unnoticeable. As a result, conditions were selected for both catalysts, under which the conversion of guaiacol was average. The recycling test of MoP was decided to carry out under the following conditions: 340 °C, 5 MPa, and 1 h (Figure 5c). Guaiacol conversion was demonstrated to reduce from 74 to 30% within five cycles, while selectivity for phenol remained constant. The recycling test of WP at average conversion was carried out at 360 °C, 5 MPa, and 3 h. Guaiacol conversion was 45% on the 1st run and decreased to 33% after the 5th run (Figure 5d). A decrease in activity was noted not only for the WP catalyst but also for MoP. However, a decrease in the activity and stability of catalysts was not shown to affect the change in phenol selectivity.

**3.4. Characterization of the Spent Catalysts.** One of the reasons for the deactivation of phosphide catalysts is the oxidation of phosphide to phosphate.[40,51−53] Another reason is coke deposition on the active sites.[43,54] Previously, the study of phosphide deactivation during the hydrodeoxygenation process was carried out in a number of works. Wu et al. made a comparison of fresh and spent $Ni_2P/SiO_2$, $Ni_2P/ZrO_2$, and $Ni_2P/Al_2O_3$ catalysts in guaiacol hydrodeoxygenation using XRD.[49] The peaks of the $Ni_2P$ phase were not shown to identify in spent catalysts. It was suggested that coke deposition or loss of some P under $H_2$-rich conditions was the cause of catalyst deactivation. Lan et al. made an investigation of the catalyst surface before and after the reaction by XPS, XRD, transmission electron microscopy (TEM), and temperature-programmed oxidation (TPO).[43] XPS showed that guaiacol or anisole hydrodeoxygenation for 48 h over $Ni_2P/SiO_2$ was found to contribute to surface nickel phosphate reduction rather than nickel phosphide oxidation. $Ni^{\delta+}$, $Ni^0$, and $P^{\delta-}$ surface content increased in a spent catalyst. Moreover, XRD showed that the $Ni_2P$ phase remained stable after 48 h of use. TEM presented a slight growth of phosphide particles. TPO indicated a significant deposition of coke on the catalyst surface after 24 and 48 h of reaction. Therefore, it was concluded that the phosphide oxidation to phosphate was not the cause of catalyst deactivation. The main factor of deactivation was coke deposition.

**Scheme 1. Proposed Pathways of Guaiacol Hydrodeoxygenation over Phosphide Catalysts**

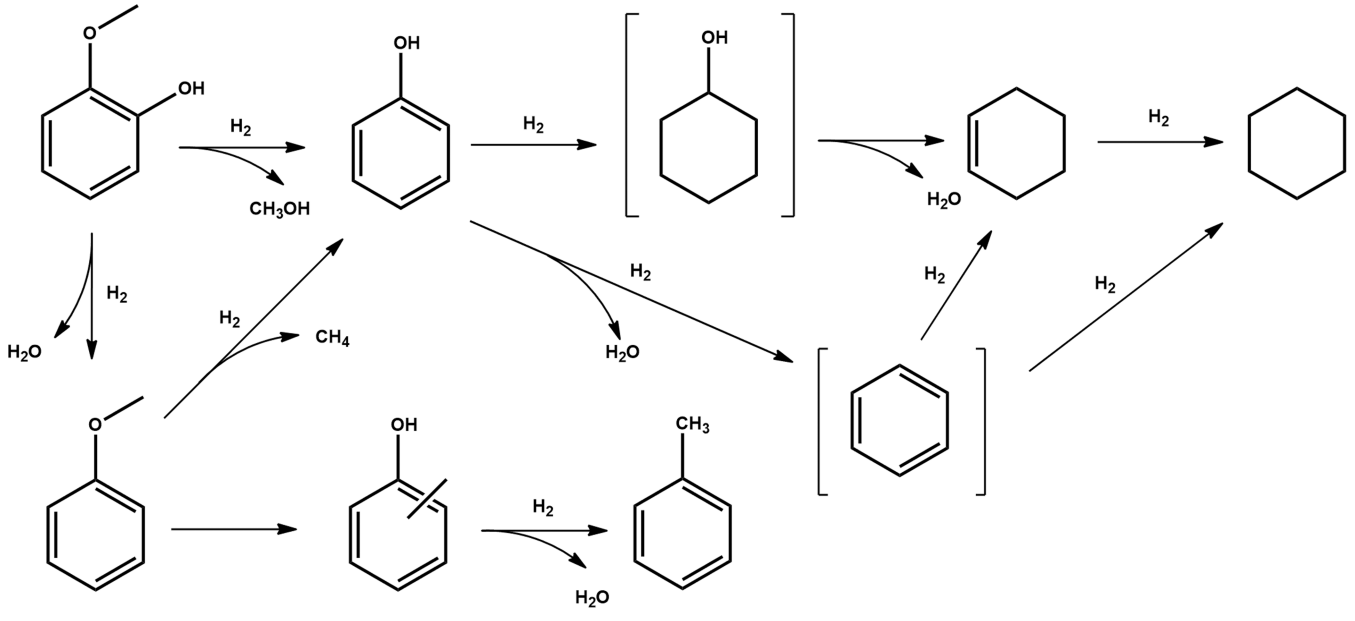




https://doi.org/10.1021/acsomega.2c06396
ACS Omega 2022, 7, 40586−40595

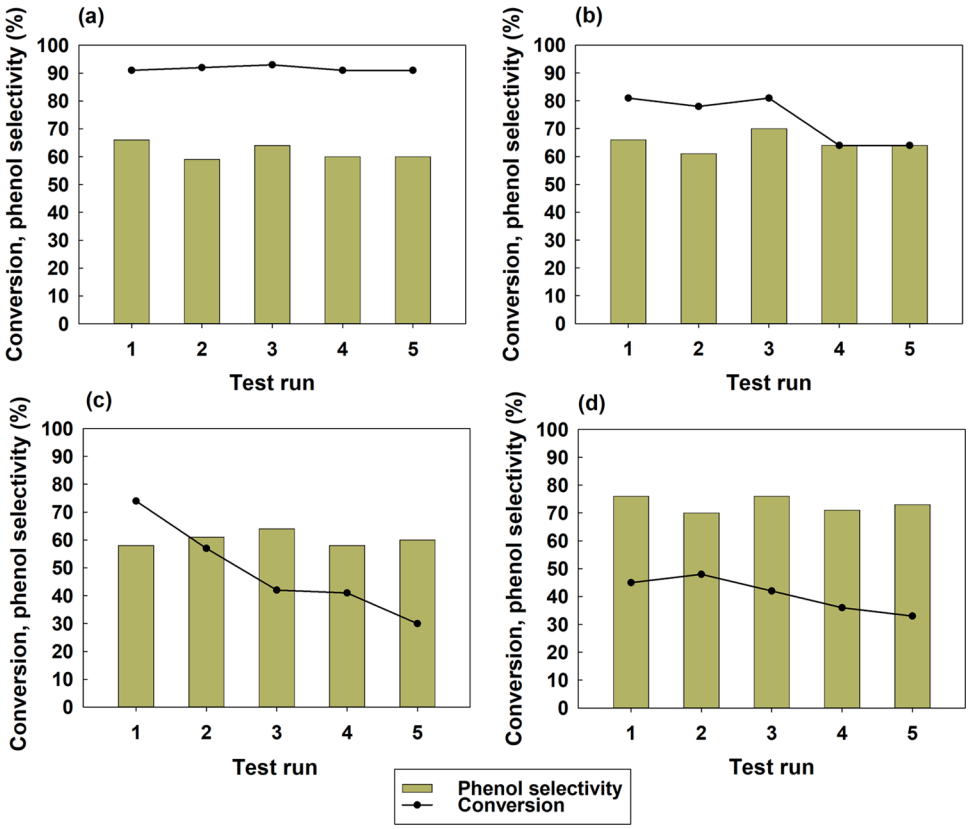


**Figure 5.** Recycling test runs of MoP under the following conditions: (a) 340 °C, 5 MPa $H_2$, 6 h and (c) 340 °C, 5 MPa $H_2$, 1 h; and WP: (b) 340°C, 5 MPa $H_2$, 6 h and (d) 360 °C, 5 MPa $H_2$, 3 h.

At the same time, de Souza et al. investigated potential coke deposition over supported nickel phosphide catalysts after phenol hydrodeoxygenation by Raman spectroscopy.[55] The characteristic bands of carbonaceous materials did not occur in the spectra of the used catalysts. Therefore, carbon deposition could not be considered the cause of catalyst deactivation.

Jiménez-Gómez et al. explored $Ni_2P/SiO_2$ deactivation after furfural hydrodeoxygenation by XRD and XPS.[54] XRD showed stability of the $Ni_2P$ phase after the reaction, while XPS presented that Ni and P decrease on the catalyst surface that the authors related to coke deposition.

Cecilia et al. mentioned $Ni_2P/SiO_2$ oxidation by water during dibenzofuran hydrodeoxygenation identified by XPS.[53] Moreover, catalysts with a lower phosphorus content were deactivated by water faster than catalysts with a higher phosphorus content.

In the present work, the catalyst deactivation was investigated by XRD and XPS. XRD analysis provided the catalyst phase composition after 30 h of operation (Figure 6). There was a decrease in the number of crystalline patterns in the MoP sample. The peaks identified were observed at $2\theta$ = 32.36, 43.34, and 57.44°, corresponding to the (100), (101), and (110) planes in MoP, respectively (PDF No. 89-5110). The evaluated average size of crystallites was 29 ± 2 nm. In the WP sample, the background/peak intensity ratio increased. The peaks identified were placed at $2\theta$ = 43.32 and 44.94°, corresponding to the (112) and (211) planes in WP (PDF No. 80-0238). The evaluated average size of crystallites was 30 ± 1 nm. The crystallite sizes of the fresh and spent catalysts were comparable; therefore, it was not possible to make a conclusion about the growth or reduction in size during

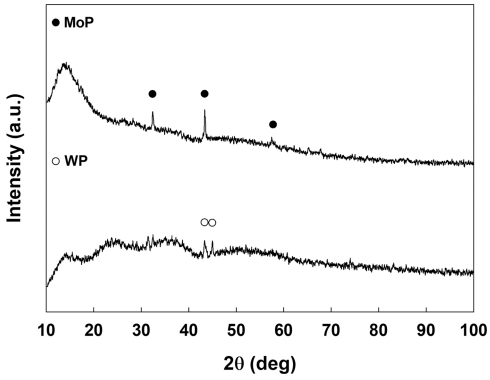


**Figure 6.** Powder X-ray diffraction of the spent molybdenum and tungsten phosphides.

guaiacol hydrodeoxygenation. However, for MoP, it can be seen that the interaction of the catalyst with water during guaiacol hydrodeoxygenation contributed to the partial destruction of the crystalline phase and, consequently, the amorphization of the catalyst. It is likely that the resulting amorphous phase can be related to phosphate, which is formed as a result of phosphide oxidation.

Since the conversion of guaiacol decreased more significantly for MoP after five test runs of 1 h than after five test runs of 6 h, the spent catalyst after 5 h of operation was also investigated. The number of peaks corresponding to the crystalline phase of MoP decreased compared to the fresh catalyst (Figure S4). Peaks were identified at $2\theta$ = 28.40, 32.52, 43.46, and 57.62, corresponding to the (001), (100), (101), and (110) planes in MoP (PDF No. 89-5110). The evaluated


https://doi.org/10.1021/acsomega.2c06396
ACS Omega 2022, 7, 40586−40595

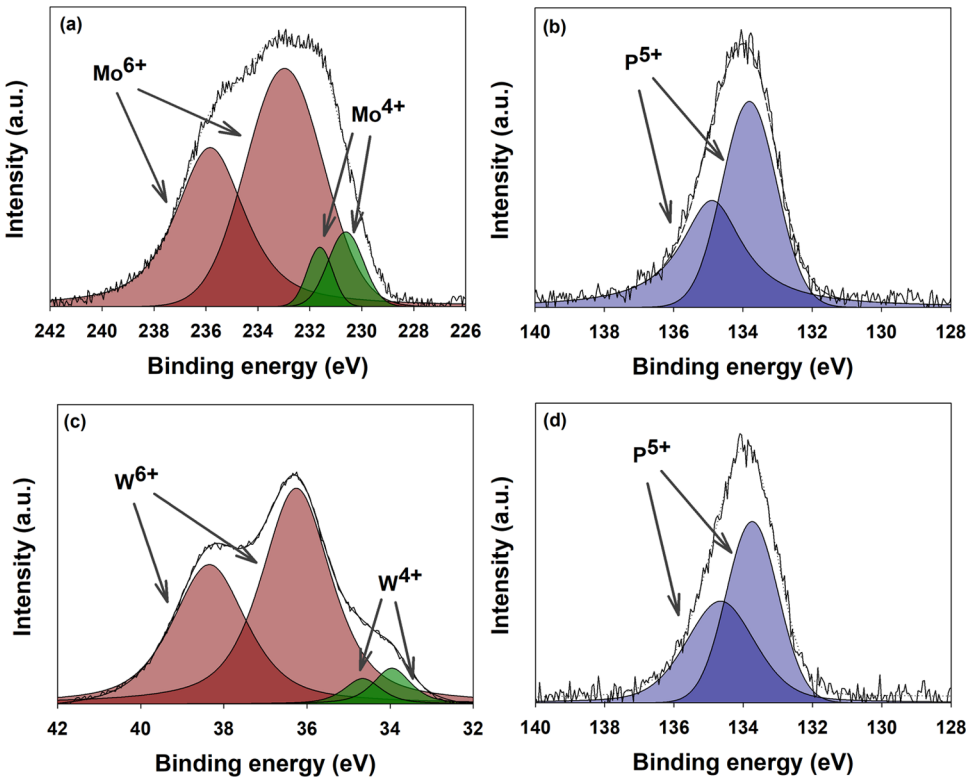


**Figure 7.** X-ray photoelectron spectra of the spent molybdenum phosphide for (a) Mo 3d and (b) P 2p regions and tungsten phosphide for (c) W 4f and (d) P 2p regions.

average size of crystallites was 30 ± 1 nm. Thus, the destruction of the crystalline phosphide phase partially occurred, but to a lesser extent than after 30 h of operation.

The XPS analysis of the spent catalysts showed that after 30 h of operation, the peaks related to metal phosphides disappeared in the spectra of both catalysts (Figure 7). There are two peaks related to $Mo^{4+}$ species in the molybdenum-containing catalyst centered at 230.6 eV ($3d_{5/2}$) and 231.6 eV ($3d_{3/2}$) and two peaks related to $Mo^{6+}$ species are centered at 233.0 eV ($3d_{5/2}$) and 235.8 eV ($3d_{3/2}$) (Figure 7a). Similarly, for a tungsten-containing catalyst (Figure 7c), peaks related to $W^{4+}$ (34.0 eV in the $4f_{7/2}$ region and 34.7 eV in the $4f_{5/2}$ region) and $W^{6+}$ (36.3 eV in the $4f_{7/2}$ region and 38.3 eV in the $4f_{5/2}$ region) are observed in the spectrum. At the same time, the content of $M^{4+}$ in the spent catalyst increased compared to its content in the fresh catalyst (Table S2). It can be assumed that $M^{\delta+}$ is oxidized to $M^{4+}$. The peaks related to $P^{\delta-}$ species (129.4−131.1 eV) in MoP and WP were also not detected in the spent catalyst spectra (Figure 7b,d). These results may be evidence of phosphide surface phase oxidation by $H_2O$, formed in guaiacol hydrodeoxygenation. Surface oxidation may cause a decrease in catalytic activity in the recycling tests.

The XPS analysis also was carried out for the spent MoP catalyst obtained after five test runs of 1 h each (Figure S5). $Mo^{\delta+}$ content decreased and $Mo^{4+}$ increased in comparison with their content in the fresh MoP (Table S3). This indicates that $Mo^{6+}$ is partially reduced to $Mo^{4+}$ at the reaction temperatures,[56] while $Mo^{\delta+}$ is oxidized in the presence of water. $P^{\delta-}$ content also decreased in comparison with its content in the fresh catalyst. Thus, both spent MoP catalysts were characterized by partial destruction of the phosphide crystalline phase and surface oxidation, which caused a decrease in catalytic activity during recycling tests.

## 4. CONCLUSIONS

The bulk molybdenum phosphide catalyst, containing the MoP phase, and the bulk tungsten phosphide catalyst, containing the WP phase, were compared in guaiacol hydrodeoxygenation for the first time. MoP was shown to be more active than WP. Guaiacol conversion using MoP was 90−98%. The highest selectivity for phenol was 66% (340 °C). With increasing temperature to 380 °C, the phenol selectivity decreased to 31%, while selectivity for cyclohexane increased to 29%. The catalyst was suggested to be active not only in hydrodeoxygenation but also in hydrogenation. Guaiacol conversion over WP was 53−90%. The highest selectivity for phenol was 84% (380 °C). Thus, WP was active in the partial hydrodeoxygenation of guaiacol and was more suitable for the selective production of phenol than MoP. The recycling test runs of the catalysts showed that MoP is more stable than WP under the same reaction conditions (340 °C, 5 MPa $H_2$, 6 h). However, at average guaiacol conversion, MoP lost its activity faster than WP. Nevertheless, a decrease in the activity did not affect the selectivity for phenol for both catalysts. There are various reasons for the decrease in the activity of phosphide catalysts, i.e., phosphide oxidation to phosphate and coke deposition on the catalyst surface. In the present work, catalyst deactivation was studied using XRD and XPS and was associated with the partial destruction of the crystalline active phase, the probable formation of amorphous phosphate, and a decrease in the phosphide content on the catalyst surface. Summing up the results of this work, phosphide catalysts can be successfully used in guaiacol transformation, but increasing their stability is of current interest.



https://doi.org/10.1021/acsomega.2c06396
ACS Omega 2022, 7, 40586−40595

## ■ ASSOCIATED CONTENT

### Supporting Information

The Supporting Information is available free of charge at https://pubs.acs.org/doi/10.1021/acsomega.2c06396.

Oxidation states on the surface of the fresh catalysts, identified by XPS (Table S1); $NH_3$-TPD desorption curves of MoP and WP (Figure S1); effect of reaction temperature on the minor product selectivity over MoP (Figure S2); effect of reaction temperature on the minor product selectivity over WP (Figure S3); powder X-ray diffraction of the spent molybdenum phosphide (five test runs of 1 h each) (Figure S4); oxidation states on the surface of the spent catalysts after 30 h of operation, identified by XPS (Table S2); X-ray photoelectron spectra of the spent molybdenum phosphide (five test runs of 1 h each) for (a) Mo 3d and (b) P 2p regions (Figure S5); oxidation states on the surface of the spent MoP after 5 h of operation, identified by XPS (Table S3) (PDF)

## ■ AUTHOR INFORMATION


### Corresponding Author

**Maria A. Golubeva** − *A.V.Topchiev Institute of Petrochemical Synthesis, RAS, Moscow 119991, Russian Federation;* orcid.org/0000-0002-3741-7833; Phone: +7 (495) 647-59-27 (309); Email: vinnikova@ips.ac.ru

### Authors

**Mariyam Mukhtarova** − *A.V.Topchiev Institute of Petrochemical Synthesis, RAS, Moscow 119991, Russian Federation*

**Alexey A. Sadovnikov** − *A.V.Topchiev Institute of Petrochemical Synthesis, RAS, Moscow 119991, Russian Federation*

**Anton L. Maximov** − *A.V.Topchiev Institute of Petrochemical Synthesis, RAS, Moscow 119991, Russian Federation*

Complete contact information is available at: https://pubs.acs.org/10.1021/acsomega.2c06396


### Author Contributions

The manuscript was written through contributions of all authors. All authors have given approval to the final version of the manuscript.


### Funding

This work was carried out within the State Program of TIPS RAS.


### Notes

The authors declare no competing financial interest.


## ■ ACKNOWLEDGMENTS

This work was performed using the equipment of the Shared Research Center Analytical center of deep oil processing and petrochemistry of A.V.Topchiev Institute of Petrochemical Synthesis RAS and the JRC PMR IGIC RAS.


## ■ ABBREVIATIONS

BTX, benzene−toluene−xylene fraction; WHSV, weight hourly space velocity; XRD, powder X-ray diffraction; XPS, X-ray photoelectron spectroscopy; SEM, scanning electron microscopy; EDX, energy-dispersive X-ray spectroscopy; $NH_3$-TPD, temperature-programmed desorption of $NH_3$; GC−MS, gas chromatography−mass spectroscopy; GLC, gas−liquid chromatography; TEM, transmission electron spectroscopy; TPO, temperature-programmed oxidation

## ■ REFERENCES


(1) Wang, S.; Dai, G.; Yang, H.; Luo, Z. Lignocellulosic biomass pyrolysis mechanism: A state-of-the-art review. *Prog. Energy Combust. Sci.* **2017**, *62*, 33−86.

(2) Bridgwater, T. Biomass for energy. *J. Sci. Food Agric.* **2006**, *86*, 1755−1768.

(3) Ragauskas, A. J.; Beckham, G. T.; Biddy, M. J.; Chandra, R.; Chen, F.; Davis, M. F.; Davison, B. H.; Dixon, R. A.; Gilna, P.; Keller, M.; Langan, P.; Naskar, A. K.; Saddler, J. N.; Tschaplinski, T. J.; Tuskan, G. A.; Wyman, C. E. Lignin Valorization: Improving Lignin Processing in the Biorefinery. *Science* **2014**, *344*, No. 1246843.

(4) Brebu, M.; Vasile, C. Thermal degradation of lignin—a review. *Cellul. Chem. Technol.* **2010**, *44*, 353−363.

(5) Wang, H.; Pud, Y.; Ragauskas, A.; Yang, B. From lignin to valuable products−strategies, challenges, and prospects. *Bioresour. Technol.* **2019**, *271*, 449−461.

(6) Miyagawa, A.; Nakagawa, Y.; Tamura, M.; Tomishige, K. Demethoxylation of hydrogenated derivatives of guaiacol without external hydrogen over platinum catalyst. *Mol. Catal.* **2019**, *471*, 60−70.

(7) Zhou, H.; Wang, H.; Sadow, A. D.; Slowing, I. I. Toward hydrogen economy: Selective guaiacol hydrogenolysis under ambient hydrogen pressure. *Appl. Catal., B* **2020**, *270*, No. 118890.

(8) Nekhaev, A. I.; Maksimov, A. L. Production of Aromatic Hydrocarbons from Biomass. *Pet. Chem.* **2021**, *61*, 16−34.

(9) Niu, X.; Feng, F.; Yuan, G.; Zhang, X.; Wang, Q. Hollow MFI Zeolite Supported Pt Catalysts for Highly Selective and Stable Hydrodeoxygenation of Guaiacol to Cycloalkanes. *Nanomaterials* **2019**, *9*, No. 362.

(10) Teles, C. A.; de Souza, P. M.; Rabelo-Neto, R. C.; Teran, A.; Jacobs, G.; Weikert, C. V.; Magriotis, Z. M.; Gonçalves, V.O.O.; Resasco, D. E.; Noronha, F. B. Reaction pathways for the HDO of guaiacol over supported Pd catalysts: Effect of support type in the deoxygenation of hydroxyl and methoxy groups. *Mol. Catal.* **2022**, *523*, No. 111491.

(11) He, Y.; Liu, R.; Yellezuome, D.; Peng, W.; Tabatabaei, M. Upgrading of biomass-derived bio-oil via catalytic hydrogenation with Rh and Pd catalysts. *Renewable Energy* **2022**, *184*, 487−497.

(12) Xin, Y.; Zheng, Z.; Luo, Z.; Jiang, C.; Gao, S.; Wang, Z.; Zhao, C. The influence of pore structures and Lewis acid sites on selective hydrogenolysis of guaiacol to benzene over Ru/TS-1. *Green Energy Environ.* **2021**, *7*, 1014−1023.

(13) Guo, X.; Wang, W.; Wu, K.; Huang, Y.; Shi, Q.; Yang, Y. Preparation of Fe promoted $MoS_2$ catalysts for the hydrodeoxygenation of p-cresol as a model compound of lignin-derived bio-oil. *Biomass Bioenergy* **2019**, *125*, 34−40.

(14) Mortensen, P. M.; Gardini, D.; Damsgaard, C. D.; Grunwaldt, J.-D.; Jensen, P. A.; Wagner, J. B.; Jensen, A. D. Deactivation of Ni-$MoS_2$ by bio-oil impurities during hydrodeoxygenation of phenol and octanol. *Appl. Catal., A* **2016**, *523*, 159−170.

(15) Wang, H. H.; Liu, Z. L.; Song, Y. C.; Li, H. High-Performance Evolution of $Ni_2P$@Hierarchical HZSM-5 as the Guaiacol Hydrodeoxygenation Catalyst. *ACS Omega* **2020**, *5*, 21330−21337.

(16) Berenguer, A.; Bennett, J. A.; Hunns, J.; Moreno, I.; Coronado, J. M.; Lee, A. F.; Pizarro, P.; Wilson, K.; Serrano, D. P. Catalytic hydrodeoxygenation of m-cresol over $Ni_2P$/hierarchical ZSM-5. *Catal. Today* **2018**, *304*, 72−79.

(17) Li, Y.; Fu, J.; Chen, B. Highly selective hydrodeoxygenation of anisole, phenol and guaiacol to benzene over nickel phosphide. *RSC Adv.* **2017**, *7*, 15272−15277.

(18) Ouyang, X.; Huang, X.; Boot, M. D.; Hensen, E. J. M. Efficient Conversion of Pine Wood Lignin to Phenol. *ChemSusChem* **2020**, *13*, 1705−1709.

(19) Inocêncio, C. V.; de Souza, P. M.; Rabelo-Neto, R. C.; Teixeira da Silva, V.; Noronha, F. B. A systematic study of the synthesis of transition metal phosphides and their activity for hydrodeoxygenation of phenol. *Catal. Today* **2021**, *381*, 133−142.
(20) Horáček, J.; Akhmetzyanova, U.; Skuhrovcová, L.; Tišler, Z.; de Paz Carmona, H. Alumina-supported $MoN_x$, $MoC_x$ and $MoP_x$ catalysts for the hydrotreatment of rapeseed oil. *Appl. Catal., B* **2020**, *263*, No. 118328.
(21) Shamanaev, I. V.; Deliy, I. V.; Gerasimov, E. Y.; Pakharukova, V. P.; Bukhtiyarova, G. A. Enhancement of HDO Activity of MoP/$SiO_2$ Catalyst in Physical Mixture with Alumina or Zeolites. *Catalysts* **2020**, *10*, 45.
(22) Akhmetzyanova, U.; Tišler, Z.; Sharkov, N.; Skuhrovcová, L.; Pelíšková, L.; Kikhtyanin, O.; Mäki-Arvela, P.; Opanasenko, M.; Peurla, M.; Murzin, D. Y. Molybdenum Nitrides, Carbides and Phosphides as Highly Efficient Catalysts for the (hydro)-Deoxygenation Reaction. *ChemistrySelect* **2019**, *4*, 8453−8459.
(23) Peroni, M.; Lee, I.; Huang, X.; Baráth, E.; Gutiérrez, O. Y.; Lercher, J. A. Deoxygenation of Palmitic Acid on Unsupported Transition-Metal Phosphides. *ACS Catal.* **2017**, *7*, 6331−6341.
(24) Chen, J.; Shi, H.; Li, L.; Li, K. Deoxygenation of methyl laurate as a model compound to hydrocarbons on transition metal phosphide catalysts. *Appl. Catal., B* **2014**, *144*, 870−884.
(25) Alvarez-Galvan, M. C.; Blanco-Brieva, G.; Capel-Sanchez, M.; Morales-delaRosa, S.; Campos-Martin, J. M.; Fierro, J. L. G. Metal phosphide catalysts for the hydrotreatment of non-edible vegetable oils. *Catal. Today* **2018**, *302*, 242−249.
(26) Zhao, H. Y.; Li, D.; Bui, P.; Oyama, S. T. Hydrodeoxygenation of guaiacol as model compound for pyrolysis oil on transition metal phosphide hydroprocessing catalysts. *Appl. Catal., A* **2011**, *391*, 305−310.
(27) Berenguer, A.; Sankaranarayanan, T. M.; Gómez, G.; Moreno, I.; Coronado, J. M.; Pizarro, P.; Serrano, D. P. Evaluation of transition metal phosphides supported on ordered mesoporous materials as catalysts for phenol hydrodeoxygenation. *Green Chem.* **2016**, *18*, 1938−1951.
(28) Whiffen, V. M.; Smith, K. J.; Straus, S. K. The influence of citric acid on the synthesis and activity of high surface area MoP for the hydrodeoxygenation of 4-methylphenol. *Appl. Catal., A* **2012**, *419*−*420*, 112−125.
(29) McEnaney, J. M.; Crompton, J. C.; Callejas, J. F.; Popczun, E. J.; Biacchi, A. J.; Lewis, N. S.; Schaak, R. E. Amorphous Molybdenum Phosphide Nanoparticles for Electrocatalytic Hydrogen Evolution. *Chem. Mater.* **2014**, *26*, 4826−4831.
(30) McEnaney, J. M.; Crompton, J. C.; Callejas, J. F.; Popczun, E. J.; Read, C. G.; Lewis, N. S.; Schaak, R. E. Electrocatalytic hydrogen evolution using amorphous tungsten phosphide nanoparticles. *Chem. Commun.* **2014**, *50*, 11026−11028.
(31) Ge, R.; Huo, J.; Liao, T.; Liu, Y.; Zhu, M.; Li, Y.; Zhang, J.; Li, W. Hierarchical molybdenum phosphide coupled with carbon as a whole pH-range electrocatalyst for hydrogen evolution reaction. *Appl. Catal., B* **2020**, *260*, No. 118196.
(32) Adam, A.; Suliman, M. H.; Dafalla, H.; Al-Arfaj, A. R.; Siddiqui, M. N.; Qamar, M. Rationally Dispersed Molybdenum Phosphide on Carbon Nanotubes for the Hydrogen Evolution Reaction. *ACS Sustainable Chem. Eng.* **2018**, *6*, 11414−11423.
(33) Jiang, Y.; Shen, Y.; Dong, J.; Tan, S.; Wei, Q.; Xiong, F.; Li, Q.; Liao, X.; Liu, Z.; An, Q.; Ma, L. Surface Pseudocapacitive Mechanism of Molybdenum Phosphide for High-Energy and High-Power Sodium-Ion Capacitors. *Adv. Energy Mater.* **2019**, *9*, No. 1900967.
(34) Yang, J.; Zhang, F.; Wang, X.; He, D.; Wu, G.; Yang, Q.; Hong, X.; Wu, Y.; Li, Y. Porous Molybdenum Phosphide Nano-Octahedrons Derived from Confined Phosphorization in UIO-66 for Efficient Hydrogen Evolution. *Angew. Chem., Int. Ed.* **2016**, *55*, 12854−12858.
(35) Watson, I. M.; Connor, J. A.; Whyman, R. Non-crystalline chromium, molybdenum and tungsten phosphate films prepared by metal organic chemical vapour deposition. *Thin Solid Films* **1991**, *201*, 337−349.
(36) Li, F.; Wang, C.; Han, X.; Feng, X.; Qu, Y.; Liu, J.; Chen, W.; Zhao, L.; Song, X.; Zhu, H.; Chen, H.; Zhao, M.; Deng, Z.; Wu, J.; Zhang, P.; Gao, L. Confinement Effect of Mesopores: In Situ Synthesis of Cationic Tungsten-Vacancies for a Highly Ordered Mesoporous Tungsten Phosphide Electrocatalyst. *ACS Appl. Mater. Interfaces* **2020**, *12*, 22741−22750.
(37) Zhang, X.; Guo, T.; Liu, T.; Lv, K.; Wu, Z.; Wang, D. Tungsten phosphide (WP) nanoparticles with tunable crystallinity, W vacancies, and electronic structures for hydrogen production. *Electrochim. Acta* **2019**, *323*, No. 134798.
(38) Tawarayama, H.; Kawazoe, H.; Hosono, H. Hydrogen permeation of tungsten phosphate glass thin films. *Solid State Ionics* **2009**, *180*, 556−559.
(39) Phillips, D. C.; Sawhill, S. J.; Self, R.; Bussell, M. E. Synthesis, Characterization, and Hydrodesulfurization Properties of Silica-Supported Molybdenum Phosphide Catalysts. *J. Catal.* **2002**, *207*, 266−273.
(40) Li, K.; Wang, R.; Chen, J. Hydrodeoxygenation of Anisole over Silica-Supported $Ni_2P$, MoP, and NiMoP Catalysts. *Energy Fuels* **2011**, *25*, 854−863.
(41) Chen, J.; Guo, T.; Li, K.; Sun, L. A facile approach to enhancing activity of $Ni_2P/SiO_2$ catalyst for hydrodechlorination of chlorobenzene: promoting effect of water and oxygen. *Catal. Sci. Technol.* **2015**, *5*, 2670−2680.
(42) Galindo-Ortega, Y. I.; Infantes-Molina, A.; Huirache-Acuña, R.; Barroso-Martín, I.; Rodríguez-Castellón, E.; Fuentes, S.; Alonso-Nuñez, G.; Zepeda, T. A. Active ruthenium phosphide as selective sulfur removal catalyst of gasoline model compounds. *Fuel Process. Technol.* **2020**, *208*, No. 106507.
(43) Lan, X.; Hensen, E.J.M.; Weber, T. Hydrodeoxygenation of guaiacol over $Ni_2P/SiO_2$−reaction mechanism and catalyst deactivation. *Appl. Catal., A* **2018**, *550*, 57−66.
(44) Gutiérrez-Rubio, S.; Berenguer, A.; Přech, J.; Opanasenko, M.; Ochoa-Hernández, C.; Pizarro, P.; Čejka, J.; Serrano, D. P.; Coronado, J. M.; Moreno, I. Guaiacol hydrodeoxygenation over $Ni_2P$ supported on 2D-zeolites. *Catal. Today* **2020**, *345*, 48−58.
(45) Sad, M. E.; Padró, C. L.; Apesteguía, C. R. Study of the phenol methylation mechanism on zeolites HBEA, HZSM5 and HMCM22. *J. Mol. Catal. A: Chem.* **2010**, *327*, 63−72.
(46) Feitosa, L. F.; Berhault, G.; Laurenti, D.; Davies, T. E.; Teixeira da Silva, V. Synthesis and hydrodeoxygenation activity of $Ni_2P/C$—Effect of the palladium salt on lowering the nickel phosphide synthesis temperature. *J. Catal.* **2016**, *340*, 154−165.
(47) Dongil, A. B.; Pastor-Pérez, L.; Sepúlveda-Escribano, A.; García, R.; Escalona, N. Hydrodeoxygenation of guaiacol: Tuning the selectivity to cyclohexene by introducing Ni nanoparticles inside carbon nanotubes. *Fuel* **2016**, *172*, 65−69.
(48) Vutolkina, A. V.; Baigildin, I. G.; Glotov, A. P.; Pimerzin, Al.A.; Akopyan, A. V.; Maximov, A. L.; Karakhanov, E. A. Hydrodeoxygenation of guaiacol via in situ $H_2$ generated through a water gas shift reaction over dispersed NiMoS catalysts from oil-soluble precursors: Tuning the selectivity towards cyclohexene. *Appl. Catal., B* **2022**, *312*, No. 121403.
(49) Wu, S.-K.; Lai, P.-C.; Lin, Y.-C.; Wan, H.-P.; Lee, H. T.; Chang, Y.-H. Atmospheric Hydrodeoxygenation of Guaiacol over Alumina-, Zirconia-, and Silica-Supported Nickel Phosphide Catalysts. *ACS Sustainable Chem. Eng.* **2013**, *1*, 349−358.
(50) Wu, S.-K.; Lai, P.-C.; Lin, Y.-C. Atmospheric Hydrodeoxygenation of Guaiacol over Nickel Phosphide Catalysts: Effect of Phosphorus Composition. *Catal. Lett.* **2014**, *144*, 878−889.
(51) Lee, Y.-K.; Oyama, S. T. Bifunctional nature of a $SiO_2$−supported $Ni_2P$ catalyst for hydrotreating: EXAFS and FTIR studies. *J. Catal.* **2006**, *239*, 376−389.
(52) Moon, J.-S.; Lee, Y.-K. Support Effects of $Ni_2P$ Catalysts on the Hydrodeoxygenation of Guaiacol: In Situ XAFS Studies. *Top. Catal.* **2015**, *58*, 211−218.
(53) Cecilia, J. A.; Infantes-Molina, A.; Rodríguez-Castellón, E.; Jiménez-López, A.; Oyama, S. T. Oxygen-removal of dibenzofuran as a model compound in biomass derived bio-oil on nickel phosphide


https://doi.org/10.1021/acsomega.2c06396
*ACS Omega* 2022, 7, 40586−40595

catalysts: Role of phosphorus. *Appl. Catal., B* **2013**, *136−137*, 140−149.
(54) Jiménez-Gómez, C. P.; Cecilia, J. A.; Moreno-Tost, R.; Maireles-Torres, P. Nickel Phosphide/Silica Catalysts for the Gas-Phase Hydrogenation of Furfural to High−Added−Value Chemicals. *ChemCatChem* **2017**, *9*, 2881−2889.
(55) de Souza, P. M.; Inocêncio, C. V. M.; Perez, V. I.; Rabelo-Neto, R. C.; Gonçalves, V. O. O.; Jacobs, G.; Richard, F.; Teixeira da Silva, V.; Noronha, F. B. Hydrodeoxygenation of phenol using nickel phosphide catalysts. Study of the effect of the support. *Catal. Today* **2020**, *356*, 366−375.
(56) Hawkins, D. T.; Worrell, W. L. Hydrogen reduction of $MoO_3$ at temperatures between 300° and 450 °C. *Metall. Mater. Trans. B* **1970**, *1*, 271−273.



https://doi.org/10.1021/acsomega.2c06396
*ACS Omega* 2022, 7, 40586−40595